In form for a swarm: programmable neutrophil swarming impacts infection outcome

Salik M. Borbora[1§], Ivanna Williantarra[1§], Giulia Rinaldi[1], Can Cui[1], Echo Yongqi Luo[1], Hazel A. Walker[1], Holly M. Craven[1,2], Auxence Desrentes[1], Nir S. Gov[1,3], Milka Sarris[1*]

Affiliations:

[1]University of Cambridge, Department of Physiology, Development and Neuroscience, Downing Site, Cambridge, CB2 3DY, UK.

[2]Roving Researcher Programme, School of Biological Sciences, University of Cambridge, United Kingdom

[3]Department of Chemical and Biological Physics, Weizmann Institute of Science, Rehovot, Israel

§ These authors contributed equally

*Correspondence to: ms543@cam.ac.uk

Abstract

Migrating cells often pattern the distribution of chemoattractants to support their accumulation in target tissues. Neutrophil swarming represents a prominent example of such self-organisation. During this process, neutrophils engage in coordinated autocrine/paracrine chemoattractant signalling that drives rapid clustering at sites of injury or infection. Whether neutrophil swarming can be regeared to influence immune outcomes is unclear. Here, we show that neutrophil swarming is subject to reprogramming after microbial experience and amenable to targeted genetic engineering with measurable effects on infection outcome. We established a model of bacterial wound infection in zebrafish, focusing on *P. aeruginosa*, an important opportunistic pathogen. We demonstrate that zebrafish larvae exposed to prior microbial experience (with non-pathogenic *E. coli*) are more resistant to subsequent wound infection by *P. aeruginosa,* in comparison to naive animals. Through live imaging and chemical perturbations, we show that these training effects are in part attributed to changes in neutrophil swarming and associated gene expression. Finally, we demonstrate that genetic enhancement of 5-lipoxygenase in neutrophils is sufficient to maximise neutrophil swarming and improve infection outcome. Together, these data suggest new routes for reprogramming neutrophil accumulation in tissues, via manipulating their ability to shape chemoattractant landscapes.

Introduction

Directed cell migration is essential for tissue development and surveillance. Guidance of migrating cells relies on interpretation of gradients of chemoattractants within tissues. Traditional mechanistic models portray migrating cells as receivers of information, responding to chemoattractant landscapes patterned by extrinsic tissue cells. However, several lines of evidence highlight an important role for self-organisation in the process, through cell-autonomous generation of chemical gradients by migratory cells[1–5]. For example, during development, migrating tissue collectives sculpt chemical gradients through asymmetric distribution of dedicated chemoattractant scavenging receptors[3,5]. In cancer metastasis, melanoma cells disperse via catabolism of ligand and local micro-gradient generation[6]. In chemotactic mazes, amoeboid cells detect dead ends using breakdown of chemoattractant[7]. During immune responses, leukocytes pattern autologous chemical gradients through chemoattractant scavenging or through autocrine/paracrine secretion[8–12]. A fundamental question raised by these observations is whether the migratory patterns of cells are intrinsically programmable, in a manner sufficient to impact disease at the tissue and organism scale.

To explore this question, we focus on the prominent paradigm of neutrophil swarming, as a self-organised migration behaviour. Neutrophils are first responders to tissue injury and infection and directly fight microbes through a variety of effector mechanisms, such as phagocytosis, secretion of antimicrobial molecules, and release of neutrophil extracellular traps (NETs)[13]. Neutrophils also produce chemokines and cytokines that influence the accumulation and function of other cells and ultimately shape the course of inflammation and disease. The recruitment of neutrophils is initially prompted by primary signals produced by tissue cells afflicted by injury or infection[13]. Thereafter, neutrophils begin to secrete further chemoattractants, generating tissue-scale gradients and/or waves of chemoattractants, which amplify the range of recruitment and determine the final magnitude of the response[8–11,14–16]. The process of neutrophil swarming is highly conserved and thought to impart functional benefits in fighting infection, particularly in the face of large and focal targets, such as wound infection or fungal invasions[9,17,18]. Specifically, swarms are characterized by rapid kinetics of recruitment and dense accumulation of neutrophils[8–11,14], which in principle would support prompt containment of pathogens, physical insulation of the pathogen-afflicted area and local concentration of antimicrobial molecules. On the other hand, neutrophil accumulation is also

known to prolong pathological inflammation when not properly regulated and resolved[13,19]. Therefore, the mechanisms and rules of organisation underlying neutrophil swarm development have important functional implications in disease.

Several conserved mechanisms have been determined that drive the initiation and evolution of neutrophil swarming. This includes the key neutrophil-derived chemoattractants driving swarm development (notably, the eicosanoid leukotriene B4 (LTB4) and the chemokine Cxcl8[8,9,14,20]), signal inducers of chemoattractant secretion (such as coordinated calcium signals[9,10,21]) as well as factors that self-limit the evolution of swarms (such as receptor desensitization and reactive oxygen species[10,22,23]). Additional contributing factors have also been described, such as damage associated molecular patterns (for example ATP and fMLP[9,11]) and cellular behaviours, such as neutrophil NETosis and target cloaking by other immune cells[20,24]. Despite the overall conservation of neutrophil swarming and associated mechanisms, the dynamics of neutrophil swarm behaviours within a given experimental system show significant heterogeneity, ranging from small, short-lived clusters, to persistent and larger clusters[9,25]. Although some of this heterogeneity can be attributed to variation in the intensity and composition of tissue-derived signals[22,24], it remains unclear whether cell-intrinsic properties account for variation in neutrophil propensity to swarm and whether these are subject to re-programming.

Immune cell gene expression and function can be re-programmed in at least two ways. The first is through experience and 'training', whereby immune cells exposed to a primary insult acquire epigenetic marks that poise their gene expression profile and responsiveness to a subsequent insult[26–28]. Neutrophils have been shown to undergo such durable training after exposure to primary infection, through epigenetic re-programming in relevant long-lived progenitors[29,29–32]. Innate immune training increases resistance to infection in a variety of tumour and infection settings and involves a range of epigenome and transcriptome changes[29,30,33,34]. Whilst it is well-established that neutrophils enhance their killing capacity and associated gene signatures after immune training[29,35–37], it remains unclear to what extent their ability to swarm can also undergo re-programming under these conditions. A second route to re-programming immune function is through genetic engineering, as exemplified in tumor immunotherapies. Specifically, chimeric antigen receptors (CAR) can be engineered in immune cells to programme their ability to recognise and kill certain tumours[38]. Whilst this has been developed to the largest extent for T lymphocytes[38], new approaches for CAR therapies are geared towards the manipulation of myeloid cells, including macrophages and

neutrophils[39–42]. However, the ability to genetically reprogramme the infiltration of immune cells to target diseased tissues remains a challenging frontier. In this context, the manipulation of self-generated gradients is a relatively unexplored but interesting route of manipulation, as it offers the potential to modify the composition of inflammatory niches through the reprogramming of ligands delivered by immune cells to the site.

Here we exploit the zebrafish as a tractable model to explore the link between cell behaviours at the microscopic with disease outcome at the whole-organism scale. We developed and characterised a model of wound infection in which neutrophil swarm heterogeneities can be visualized in real time in individual animals, concomitant with monitoring of disease progression and infection outcome. We first establish factors that determine susceptibility of wound infection, notably the role of osmotic surveillance programmes in the epithelial barrier. We then show that training challenge of zebrafish with non-pathogenic microbes enhances resistance to subsequent wound infections and that, under these conditions, neutrophils exhibit enhanced swarming prowess with reduced swarm heterogeneity across individuals. We found that this correlates with upregulation of swarm-related gene expression signatures and that inhibition of swarm machinery (LTB4 biosynthesis pathway) limits the protective effects of prior microbial insult. Finally, we show that targeted genetic enhancement of swarm machinery enhances neutrophil swarming and resistance to wound infection, indicating that neutrophil swarm reprogramming is sufficient to influence infection outcome.

133 # Results

134

135 **Tissue damage detection through osmotic surveillance shapes susceptibility of zebrafish**
136 **larvae to pathogenic wound infections**

137

138 To investigate the dynamics and functional consequences of neutrophil swarms, we employed
139 a wound infection model. *Pseudomonas aeruginosa* is an opportunistic bacterial pathogen,
140 present in water and soil, able to colonise wounds in multiple species. In humans, wound
141 infections can occur through contact of injured tissue with contaminated water or surfaces[43,44].
142 These infections can be severe and lead to sepsis and mortality, particularly in
143 immunocompromised individuals or in the case of large surgery-associated infections[43,44]. We
144 previously introduced a model whereby zebrafish larvae are subjected to wounding in the
145 presence of aqueous medium contaminated with *P. aeruginosa* PAO1 strain[9]. This experimental
146 model is advantageous in that it recapitulates a natural route of infection, in comparison to
147 more common microinjection routes[45], and provides a relevant setting to study the role of
148 neutrophil swarming in defence. However, these experimental infections are inherently more
149 variable, since heterogeneities in the injured tissue can influence the titres of microbial
150 colonisation and the ensuing immune response.

151

152 To understand and control sources of variation in this model, we examined known aspects of
153 the tissue response to damage. Previous studies have shown that damage detection through
154 osmotic surveillance is important for epithelial wound closure[46], inflammatory signal
155 production and recruitment of neutrophils[47]. In addition, these tissue damage detection
156 pathways were shown to promote optimal defence from microbes, when the latter are
157 microinjected into hosts[48]. We therefore aimed to establish whether wound infections are
158 influenced by osmotic surveillance pathways, with a view to minimising variation in infection.

159

160 To test the role of osmotic surveillance, we subjected zebrafish larvae to two types of
161 wounding, mechanical and laser wounding **(Fig. 1A, G)**, in two common zebrafish buffers E3
162 medium (hypotonic), Ringer medium (isotonic), as well as isotonic E3 medium (with the same
163 sodium levels and tonicity as Ringer). The use of two wounding assays offers complementary
164 advantages. Whilst mechanical wounding can be performed on a large scale, to screen for
165 disease phenotypes, laser wounding permits real-time visualisation of neutrophil responses

166 immediately upon wounding[9,49]. In both types of wound assays, we found that larvae in
167 hypotonic medium were largely resistant to wound infection, whereas larvae in isotonic
168 medium (iso E3, Ringer) were susceptible **(Fig. 1E, H)**. In all media conditions, non-wounded
169 larvae were resistant to infection, confirming the wound-dependent nature of infection **(Fig.**
170 **1E, H)**. To characterise the disease progression in a more granular fashion, we created a disease
171 scoring matrix, with phenotypes ranging from alterations in swimming behaviour, to more
172 extensive morphological abnormalities **(Fig. 1B)**. Larvae infected in hypotonic media showed
173 minimal disease symptoms and bacterial burdens in comparison to larvae infected in isotonic
174 media (**Fig 1C, J)**.
175
176 Wound closure can be delayed in isotonic media due to lack of tissue damage detection by the
177 ruptured epithelium[46]. We hypothesised that this may render wounds more permissive to
178 bacterial colonisation, contributing to the increased burden of infection in these conditions
179 **(Fig. 1D, I)**. To test whether early wound colonisation might differ in the different media, we
180 measured bacterial burden shortly after wound infection (10 min and 30 min), at time points
181 shorter than the duplication time of *P. aeruginosa*[50]. We found that at this early stage the
182 bacterial titres were already significantly higher in isotonic conditions, suggesting either a
183 difference in bacterial colonisation or a difference in the early containment by immune cells
184 **(Fig. 1F)**. To test direct effects of the medium composition on the growth of bacteria, we
185 examined the growth of PAO1 bacteria in hypotonic E3, isotonic E3, Ringer and PBS solutions.
186 We found comparable bacterial growth after 30 min exposure in the different media, suggesting
187 that the disease phenotypes of the larvae depended on the host response **(Fig. S1)**.
188
189 Together these results suggested a role for osmotic surveillance in wound defence and allowed
190 us to establish the optimal conditions for recapitulating wound infection and associated disease
191 in larvae.
192
193 **Training through prior non-pathogenic microbial challenge alters neutrophil swarm-**
194 **related gene expression and enhances resistance to wound infections**
195
196 We thereafter used the susceptible model of wound infection (isotonic conditions for
197 infection/Ringer solution) to explore whether we can reprogramme the innate immune response
198 to infection through training. To mimic vaccination challenge, we used superficial
199 microinjection as a route. We injected non-pathogenic, CFP-expressing *Escherichia coli*

200 MG1655[51] in the otic vesicle at 2 days post-fertilisation **(Fig. 2A)**. We found this pre-challenge
201 increased the resistance to wound infection by *P. aeruginosa*, two days after the first challenge,
202 as compared with controlled PBS-pre-challenged larvae **(Fig. 2B)**. Notably, in the absence of
203 wounding, larvae were not susceptible to infection in either PBS *or E. coli*-pre-challenge,
204 confirming again the opportunistic nature of infection **(Fig. S2A)**. Varying the dose of *E. coli*
205 injection showed that a minimum dose was required to trigger protective effects **(Fig. S2B)**.
206 One way of distinguishing innate immune 'training' from immune 'priming' is by assessing
207 whether the protective effects persist after the immune response to the first challenge has passed
208 its peak or resolved. To explore the nature of the protection observed, we determined the
209 resolution kinetics of the first challenge, by measuring titres of *E. coli* and levels of
210 inflammatory cytokines **(Fig 2E)**. Both markers indicated that the response to *E. coli* had
211 largely subsided by the time the second challenge was given **(Fig 2F-J)**.
212
213 Neutrophil training is characterised by changes in transcriptomic and epigenetic signatures in
214 differentiated neutrophils and progenitors[32]. Since the training challenge led to resistance of
215 infection in a heterologous tissue site (tail versus ear), we hypothesised neutrophils from
216 hematopoietic sites might be centrally altered. To explore this, we isolated neutrophils from the
217 caudal hematopoietic tissue (CHT) **(Fig. 2K)** and found that CHT-derived neutrophils showed
218 increased expression of genes associated with inflammation and cell migration, in particular
219 *cxcl8a*, *5-lo* and cytoskeletal proteins, such as *tubg1* **(Fig 2L-R)**. This suggested that
220 neutrophils may be centrally altered by training in a manner that changes their gene expression
221 profile.
222
223 Together, these analyses revealed that innate immune responses to wound infections can be
224 trained by prior microbial challenge and suggested that, among the many likely effects of
225 training, neutrophil genes associated with cell migration (cytoskeletal proteins) or swarming
226 (autologous chemoattractant ligands) can be subject to reprogramming.
227
228 **Neutrophil swarming is enhanced through prior training challenge, and these phenotypic**
229 **changes contribute to disease resistance**
230
231 The changes in gene expression patterns in neutrophils upon training suggested that their
232 migratory behaviour is altered. To relate neutrophil swarm patterns with disease outcome, we
233 combined early imaging of wound infections (0-2 hours post infection-hpi) with monitoring of

234 disease outcome over a longer timescale (up to 24 hpi) in the same larvae **(Fig. 3A)**. We
235 confirmed that in this laser-wound assay, PBS pre-challenged, control fish were more
236 susceptible to PAO1 infection than *E. coli* pre-challenged fish **(Fig. S3A)**. We then compared
237 the behaviour of neutrophils upon wounding and found that in PBS-pre-challenged, control
238 animals, neutrophils exhibited both small-scale clustering and large-scale clustering **(Fig. 3B,**
239 **Video S1)**. By contrast, in *E. coli*-pre-challenged animals, we observed a more consistent scale
240 of clustering **(Fig. 3B, Video S2)**. To relate swarm variation to disease outcome, we plotted the
241 scale of neutrophil recruitment (number of cells at 2 hpi) versus the bacterial burden (number
242 of CFU at 24 hpi) in individual larvae. We confirmed that the initial number of neutrophils in
243 the field of view in PBS versus *E. coli*-pre-challenged fish was not significantly different **(Fig.**
244 **S3B)**. However, PBS-pre-challenged fish were characterised by greater variation in neutrophil
245 recruitment, higher disease scores and bacterial counts in comparison to *E. coli*-challenged fish
246 **(Fig. 3C)**. To understand these variations further, we stratified fish into four categories: i) weak
247 neutrophil recruiters with high bacterial burden (Group 1, G1, in **Fig. 3C**), ii) strong recruiters
248 with high bacterial burden (Group 2, G2, in **Fig. 3C**), iii) strong recruiters with weak bacterial
249 burden (Group 3. G3, in **Fig. 3C**) and iv) weak recruiters with weak bacterial burden (Group
250 4, G4, in **Fig. 3C**). We considered as 'strong recruiters' those larvae in which the cell number
251 exceeded 10 neutrophils. This was based on the distribution of the numbers seen in our
252 experiments and on previous papers indicating a minimal number of clustering neutrophils to
253 correlate with swarming kinetics of recruitment[15,16,52]. We considered as 'high burden', the
254 lowest level of CFU count at which disease symptoms were observed across all experiments
255 with these two groups of larvae. The number of larvae within G4 did not differ between PBS
256 and *E. coli*-pre-challenged fish, and we reason this group may represent larvae in which
257 bacterial colonisation was weak, as there was neither evidence for neutrophil recruitment nor
258 bacterial burden. Most notably, we found that upon *E. coli* training there was a significant
259 increase of larvae in G3 and a decrease in G1 **(Fig. 3D)**. This suggested that in a proportion of
260 control larvae (G1), the swarm potential of neutrophils is sub-maximal and limits resistance to
261 infection, whereas in *E. coli*-trained larvae, the swarm potential is maximised across different
262 animals.
263
264 As an additional analysis, we measured the maximal rate of neutrophil recruitment across the
265 2 h imaging window. Here, we plotted the number of new neutrophils arriving at the wound
266 over time and determined the slope of the curve during the phase of maximal recruitment **(Fig.**
267 **S3C, D)**. We then plotted the maximal rate of recruitment against the bacterial burden for the

same embryo. Here, we observed a trend for higher rates of recruitment in *E. coli*-pre-challenged larvae and lower burdens compared with PBS controls. We performed similar stratification of larvae, considering 'fast recruiters' and 'slow recruiters' as those that had a maximal rate of recruitment of either above or below the mean maximal rate, respectively, across all larvae in both PBS and *E. coli*-pre-challenge groups. This analysis indicated a trend for a higher probability of larvae to show fast maximal rate of recruitment and low bacterial burden **(Fig. S3D)**, although the difference was not found to be significant with this sample size **(Fig. S3E)**.

To investigate whether a change in neutrophil swarm potential contributes to wound infection resistance, we used a specific inhibitor for 5-lipoxygenese (5-LO), zileuton, to target the production of the swarm-driving chemoattractant, LTB4. When fish were wounded and infected in the presence of zileuton, the *E. coli*-pre-challenged fish did not show as marked an increase of infection resistance (over PBS-pre-challenged fish), in comparison to when control vehicle (DMSO) was used **(Fig. 3E-H)**.

Together, these results indicated that innate immune training leads to changes in neutrophil swarm patterns upon secondary pathogenic challenge, which in turn influence the probability to resolve infection successfully.

5-lipoxygenase enhancement in neutrophils is sufficient to enhance neutrophil swarming and resistance from wound infection

To determine whether reprogramming of neutrophil swarming is sufficient to influence wound infections, we used genetic engineering of 5-LO in neutrophils. We hypothesised that neutrophils expressing maximal levels of 5-LO would have enhanced swarming capacity and that this may contribute to containment of infection. We first compared the resistance to mechanical wound infection in transgenic larvae in which neutrophils overexpress 5-LO ('5-LO-Neu'; for 5-lipoxygenase overexpressing neutrophils) versus control wild type larvae. We found that 5-LO-Neu larvae showed enhanced resistance to infection, as measured by an improvement in survival rates, disease score and bacterial burden **(Fig. 4A-C)**.

To relate neutrophil swarm patterns to disease susceptibility, we combined again live imaging during the early stage of wound infection, with subsequent monitoring of disease progression

302 in individual larvae, using 5-LO-Neu transgenic larvae crossed with GCaMP-expressing
303 neutrophils. As with our mechanical wound model, we found that the 5-LO-Neu larvae showed
304 greater resistance to infection in our laser wound infection model **(Fig. S4B)**. By observation
305 of the videos, we noted heterogeneity in swarm magnitude across control larvae, which
306 appeared to be less pronounced in 5-LO-Neu larvae **(Fig. 4D** and **Videos S3** and **S4**). This was
307 not explained by developmental differences in the number of the cells, as the number of
308 neutrophils in the field of view at the start of the videos was comparable **(Fig. S4C)**. To quantify
309 these differences, we again used the number of recruited neutrophils or the maximal rate of
310 recruitment as a measure of recruitment magnitude and speed respectively. Accordingly, we
311 stratified fish into four groups: i) weak or slow neutrophil recruiters with high bacterial burden
312 (Group 1, G1, in **Fig S4D** and **Fig. 4E**, respectively), ii) strong or fast recruiters with high
313 bacterial burden (Group 2, G2, in **Fig. S4D** and **Fig. 4E**, respectively), iii) strong or fast
314 recruiters with weak bacterial burden (Group 3. G3, in **Fig. S4D** and **Fig. 4E**, respectively) and
315 iv) weak or slow recruiters with weak bacterial burden (Group 4, G4, in **Fig. S4D** and **Fig. 4E**,
316 respectively). We found that in control larvae, the main outcomes were in groups G1 and G2
317 whereas in 5-LO-Neu larvae there was increased proportion of outcomes in group G3 and a
318 decrease in group G1. Similar trends were observed whether we used the number of cells
319 recruited or the maximal rate of recruitment **(Fig. 4E and Fig. S4D)**, but the results reached
320 statistical significance only in the latter case **(Fig. 4F)**.
321
322 Together these results suggested that 5-LO enhancement in neutrophils is sufficient to enhance
323 neutrophil swarming rates and that this can provide a beneficial outcome in a subset of larvae.
324

325 # Discussion

326

327 Here, we examine the influence of neutrophil swarming on infection outcome and the extent to
328 which this migratory behaviour can be reprogrammed to alter disease outcome. We show that
329 neutrophil swarming and the expression of genes for swarm machinery are altered during
330 natural reprogramming ('training') by microbial experience. Through chemical inhibition, we
331 found that these alterations contribute to the enhanced resistance of trained animals to
332 pathogenic infection. Finally, we show that genetic engineering of 5-LO in neutrophils is
333 sufficient to accelerate neutrophil swarming and improve bacterial clearance and disease
334 progression.

Whilst exploring tissue variables influencing bacterial wound infection, we found that osmotic surveillance during tissue damage plays a major role in resistance to opportunistic wound infection. This extends findings reported previously, using *P. aeruginosa* microinjection in the context of wound infection[48]. Previous studies conversely reported that damage detection through osmotic surveillance compromised *Candida albicans* wound infection outcome[53]. Mechanistically, this was attributed to keratinocyte movement in response to hypotonic medium detection, which, rather than limiting microbial colonisation, appeared to favour tissue spreading of *C. albicans*. These discrepancies suggest that the role of osmotic surveillance in wound infection outcome depends on the type of invading microbe. For example, *P. aeruginosa* bacteria are highly mobile[54] and thus may rely less on host tissue movements for spreading than *C. albicans*.

We observed improved resistance to bacterial wound infection after a pre-challenge with non-pathogenic heterologous bacteria. These protective effects were present at a stage when the primary challenge had largely resolved, consistent with innate immune training. A limitation here is that we have not profiled the epigenetic signatures of neutrophils or sampled the resistance effects at longer time scales. However, other studies have shown that zebrafish neutrophils undergo epigenetic modifications during training with *Shigella flexneri* (which are phylogenetically close to *E. coli)* in a comparable timeframe with our study[37]. In addition, other studies have demonstrated that neutrophil training in zebrafish larvae arises through changes in hematopoietic stem cells within similar timeframes post-infection, as has been reported in adult mammals[35]. Our observations are consistent with such central reprogramming of neutrophils, as the protective effects were seen across heterologous tissue sites and the gene expression changes were detectable in neutrophils isolated from hematopoietic tissue. Though the detailed mechanisms remain to be investigated, our study highlights novel routes for training in wound infection settings. Probiotic *E. coli* strains have been reported to have beneficial effects on viral resistance in mouse models[55], but to our knowledge such training has not been reported for wound infection.

We found that neutrophil swarm capacity is amenable to reprogramming after microbial experience. Specifically, neutrophils upregulated expression of genes associated with swarming and larvae were less likely to show poor swarming and high susceptibility to infection. Whether these larvae represent a biologically distinct group of ‘less trained’ larvae

369 or part of a normal distribution is difficult to ascertain with this experimental size. However, it
370 is interesting to note that individual variations in training have been reported in humans
371 exposed to Bacillus Calmette-Guérin (BCG) vaccine, wherein training improved outcome in a
372 subpopulation of individuals with sub-maximal immunological profiles at the time of
373 vaccination[56]. Another noteworthy observation in our data was that training reduced the
374 higher-end values for swarm kinetics (with migration kinetics more closely clustered around a
375 medium range). One potential explanation is that the effect of increasing neutrophil numbers
376 has non-linear effects on bacterial clearance, whereby at low neutrophil numbers the changes
377 in neutrophil kinetics can make a significant difference in bacterial clearance whereas beyond
378 a certain number of recruited neutrophils, the benefit decreases. A question raised is why
379 neutrophil swarming has not evolved to be maximal regardless of immune experience and
380 whether it is detrimental to have high levels of swarm machinery. We speculate that adaptive
381 reprogramming of neutrophil swarming may reflect a strategy to economise energy or a means
382 to balance the risks of overt inflammation.
383
384 Our discovery that engineering 5-LO is sufficient to improve bacterial clearance has relevance
385 to cellular immunotherapies. Strategies for genetic modification of immune cells are growing
386 and extending to cell types beyond lymphocytes, due to advances in genetic engineering and
387 stem cell biology[39,40,42,57]. In this backdrop, the engineering of chemoattractant receptors has
388 been conceptualised to improve the efficacy of CAR-engineered immune cell deployment to
389 tumors[58]. Our study suggests that harnessing the ability of immune cells to seed
390 chemoattractant gradients in target tissues may offer new routes for reprogramming immune
391 cell migratory patterns.
392
393
394

Acknowledgements

The *P. aeruginosa* strains were kindly provided by Prof. Martin Welch, Department of Biochemistry, University of Cambridge and the *E. coli* strains were kindly provided by Dr. Somenath Bakshi, Department of Engineering, University of Cambridge. S.M.B., I.W., G.R., C.C., Y.L. were supported by the European Research Council (ERC) under the Horizon 2020 program and UKRI, Grant agreement No. EP/Y02799X/1. Y.L. is also supported by a BBSRC DTP programme BB/X010899/1. N.S.G acknowledges support from the Royal Society Wolfson Visiting Fellowship RSWVF\R2\2320010. H.A.W. was supported by an MRC DTP studentship (MR/N013433/1) and a Leverhulme Trust grant (RPG-2021-226). H.M.C. was supported by the Roving Researcher scheme in the School of Biological Sciences, University of Cambridge. A.D. was supported by a MIRES scholarship from IdEx Université Paris Cité ANR-18-IDEX-0001, funded by the French Government through its 'Investments for the Future' program. The authors gratefully acknowledge the Cambridge Imaging Centre for their support and assistance in this work.

Competing Interests

The authors declare no competing interests

Methods

Experimental model and subject details

All zebrafish were maintained in accordance with UK Home Office regulations under the UK Animals (Scientific Procedures) Act 1986 (PPL number PP4458156), with approval from the University Biomedical Service Committee. Adult fish were maintained and bred following established protocols[59]. Briefly, zebrafish were bred and maintained under standard conditions at 28.5 ± 0.5 °C on a 14 h light:10 h dark cycle. Embryos were collected from natural spawnings at 3 hours post-fertilization (hpf), bleached for 5 minutes in 0.003% sodium hypochlorite (NaOCl; Cleanline, CL3013), and rinsed three times with E3 medium. They were subsequently incubated at 28 °C in E3 medium supplemented with 0.1 µg /ml methylene blue (Sigma-Aldrich, M9140-25G). For imaging experiments, E3 medium was additionally supplemented with 0.003% 1-phenyl-2-thiourea (PTU; Sigma Aldrich, P7629) to inhibit pigmentation and preserve optical transparency.

For experiments that required *E. coli* training, *E. coli* was administered to larvae at 2 days post-fertilization (dpf) and subsequent re-challenge experiments were done at the 4 dpf stage. In experiments without training, larvae at 3-4 dpf were used. For live imaging, larvae were anesthetized in appropriate buffer containing 160-200 mg/L MS-222 (Sigma-Aldrich, E10521-50G). Where indicated, larvae were treated with Zileuton (20 µM, Tocris, 3308) or appropriate volume of vehicle (DMSO (Sigma-Aldrich, 276855-100ML)) solution by immersion.

The following transgenic zebrafish lines were used: Tg(*lyz*:GCamp6F)^{cu104} and Tg(*lyz:*tRFP-5LO) ^{cu106} from previously described work[9] ,Tg(*mpx*:GFP)i114[60], Tg(*runx1+23*:mCherry).

Bacterial culture and preparation

For *E. coli* injection, cyan fluorescent protein (CFP)-expressing *E. coli* MG1655 7740 strain was developed as described previously[61]. A single colony was obtained from a four-way streak on antibiotic-free LB Agar (Melford, A20020-500.0) plate. The colony was inoculated into 50 ml of antibiotic-free LB broth (Formedium, LBX0102) and cultured at 37 °C with shaking until the OD_{600} reading reached 0.8-0.9. The culture was then aliquoted into 1 ml stocks in antibiotic-free LB broth with 20% v/v glycerol (Fisher Scientific, G/0650/17), snap-frozen with liquid nitrogen, and stored at -80 °C until usage. On the day of the experiment, aliquots of *E. coli* were thawed at 37 °C, pelleted by centrifugation at 5,000 × *g* for seven minutes at 4 °C, and

446 washed twice with PBS (Sigma Aldrich, D8537). The bacteria were finally suspended in PBS
447 with 10% v/v phenol red (Sigma, P0290).
448 For *P. aeruginosa* infection, PAO1 strain was used[9]. One day prior to infection, a single colony
449 of *P. aeruginosa* was obtained from a four-way streak on Pseudomonas Isolation Agar (PIA;
450 BD Difco, 292710) supplemented with cetrimide and nalidixic acid (E&O Laboratories Ltd,
451 LS0006) and glycerol. The colony was inoculated into 5 ml of antibiotic-free LB broth and
452 cultured at 37 °C with shaking for 24 h. On the day of the experiment, the overnight culture
453 was diluted in fresh LB and incubated to mid-logarithmic phase (OD_{600} = 0.6–0.8). Bacterial
454 density was adjusted to 3×10^5 CFU/mL using spectrophotometric estimation. Bacteria were
455 pelleted at 1700 × *g* for five minutes and washed twice with PBS to remove residual growth
456 medium, then resuspended in PBS.
457
458 **PBS and *E. coli* injections**
459 On the day of injections, *E. coli* injection mix was prepared as described above. PBS injection
460 mix was prepared as PBS with 10% v/v phenol red for control. Larvae were anaesthetised in
461 E3 medium supplemented with 0.1 µg/ml methylene blue and 160-200mg/L MS-222. The left
462 otic vesicle of each zebrafish larva was then injected with 2 drops of 0.125 nL of PBS or *E.*
463 *coli* injection mix with a pressure of 20 psi using Picospritzer III microinjector (Intracell), as
464 previously described[62]. To confirm the dose of *E. coli* injected, 2 drops of 0.125 nL of injection
465 mix was directly injected into a microcentrifuge tube containing 100 µl PBS after the injections
466 and were then plated onto antibiotic-free LB Agar plates overnight at 37 °C at 10^0 and 10^{-1}
467 dilution. The bacterial colony forming units (CFU) were then determined by counting the
468 number of CFP^+ colonies after overnight incubation. Only when the *E. coli* injection dose
469 exceeded 400 CFU/ml were the larvae included for subsequent experiments. After injections,
470 larvae were transferred to fresh E3 medium supplemented with 0.1 µg/mL methylene blue and
471 kept at 28 °C until further use.
472
473 **Tail transection, wound infection and survival assay**
474
475 Zebrafish larvae were transferred to a Petri dish containing Ringer's solution and 160-200 mg/L
476 MS-222. Tail transection was done using a surgical blade (Swann Morton, 0510) at the distal
477 boundary of the notochord, avoiding injury to the notochord. Non-transected larvae served as
478 controls. Immediately after tail transection, larvae were transferred to a six-well plate
479 containing Ringer's solution with 3×10^5 CFU/mL *P. aeruginosa* (for the role of specific

480 buffers, E3/isotonic E3/Ringer were used as indicated) and incubated at 32 °C for 3 h. After
481 incubation, larvae were washed five times in E3 medium (without methylene blue). Individual
482 larvae were then placed in wells of a 24-well plate containing 1 mL E3 (without methylene
483 blue) and monitored for survival and disease progression. For 5-LO inhibition assays, 20 μM
484 zileuton treatment (diluted in DMSO) was initiated 1 h prior to tail transection and maintained
485 until the end of the experiment.
486
487 Survival was assessed immediately after washing, at 3 hpi, and 24 hpi. Assessment was also
488 done at intermediate time points (7 hpi and 10 hpi) when experiment was done for 24 h. For
489 48h time point experiments, analysis was done at 3 h, 24 h and 48 h. Phenotypic disease scoring
490 was done on a 0–4 scale **(Fig. 1B)** based on behavioural responses, transparency, tissue
491 integrity, circulation, and survival. Between observation timepoints, larvae were returned to 32
492 °C. A score of 4 was defined as death of the organism that was determined by the absence of
493 heartbeat as observed under the microscope.
494
495 **Bacterial burden quantification**
496 At indicated timepoints, zebrafish larvae from each condition were pooled into groups of three
497 larvae and homogenised in 300 μL PBS containing 0.1% v/v Triton X-100 (VWR, 28817.295)
498 using sterile pestles. Serial dilutions (up to 10^{-3}) were prepared in PBS and plated on PIA
499 supplemented with cetrimide and nalidixic acid (as per manufacturer's instructions) for *P.*
500 *aeruginosa* or antibiotic-free LB agar for *E. coli.* CFU were then counted after 24 hours
501 incubation.
502
503 **Fluorescence-Activated Cell Sorting (FACS)**
504 Approximately 400 embryos from a cross between Tg(*mpx*:GFP)^{i114} and
505 Tg(*runx1+23*:mCherry) transgenic lines were injected with either *E. coli* or PBS (200 per
506 group) in the otic vesicles at 2 dpf as described above. At 4 dpf, larvae were collected into
507 microcentrifuge tubes, rinsed twice with 1x HBSS (prepared by diluting 10x HBSS (Gibco™,
508 14175095) in UltraPure™ DNase/RNase-Free Distilled Water (Invitrogen™, 10977035)), and
509 placed on ice for 10 minutes to immobilise the larvae. The caudal haematopoietic tissue (CHT)
510 regions from the larvae were dissected on sterile petri dishes using ethanol-sterilised scalpels
511 and centrifuged to remove excess HBSS.
512 For tissue dissociation, 500 μL of digestion solution (2% w/v collagenase (Gibco™, 17104019)
513 and 40% v/v trypsin (Gibco™, 15400054) in 1x HBSS) was added to each tube. Samples were

514 incubated at 30 °C for 30 minutes with periodic trituration by pipetting. Digestion was halted
515 with 1x HBSS containing 10% v/v heat-inactivated fetal bovine serum (FBS; Gibco™,
516 A5670701). All subsequent steps were performed on ice. Cells were centrifuged at 500 × g for
517 5 minutes at 4 °C and then resuspended in sorting solution (1x HBSS supplemented with 10
518 mM HEPES 15630056) and 2% FBS) and filtered through a pre-wetted 40 µm cell strainer
519 (Falcon, 352340). Filtered cells were centrifuged and resuspended in 1 ml sorting solution in a
520 microcentrifuge tube. Cell viability and concentration were assessed using trypan blue (Gibco,
521 15250) staining and a hemocytometer, respectively.
522 GFP-positive neutrophils were FAC-sorted using a BD FACS Aria III (Becton Dickinson)
523 directly into 100 µL of lysis solution supplied with the RNAqueous® Micro Kit (ThermoFisher,
524 AM1931).
525
526 **RNA extraction and cDNA synthesis**
527 For transcriptomic analysis, RNA isolation was done from the sorted cells using the
528 RNAqueous® Micro Kit (Thermo Fisher, AM1931) according to the manufacturer's
529 instructions, including DNase I digestion step to eliminate genomic DNA contamination.
530
531 For cytokine expression analysis following PBS/ *E. coli* injections, at 2 dpf, RNA was extracted
532 from groups of 10 wild-type zebrafish per condition (non-injected, PBS-injected, and *E. coli*-
533 injected) after euthanasia with MS-222 at 4.5 hours post-injection using the RNeasy® Mini Kit
534 (Qiagen, 74104). Subsequently, from 3 to 10 dpf, groups of 8-10 larvae per condition were
535 euthanised with MS-222 prior to RNA extraction.
536
537 The obtained RNA concentrations were measured using the Nanodrop. Purified RNA was then
538 reverse transcribed into cDNA using the Maxima H Minus First Strand cDNA Synthesis Kit
539 (ThermoFisher, K1651) following the manufacturer's protocol. Finally, cDNA was stored at -
540 20 °C until further use for quantitative PCR (qPCR) analysis.
541
542 **Gene expression analysis by qRT-PCR**
543
544 The qRT-PCR was performed using the PowerTrackTM SYBR™ Green Master Mix
545 (ThermoFisher, A46012) and carried out in the LightCycler® 480 Instrument II (Roche). For
546 transcriptomic analysis, each reaction contained 0.5 ng of cDNA, 10 nM of primer pairs, and
547 1X master mix. The zebrafish gene *rpl32* served as the reference for normalisation.

548 For cytokine expression analysis, each reaction contained 5 ng cDNA, 500 nM primer pairs,
549 and 1X master mix and the zebrafish gene *ef1a* served as the reference for normalisation.
550 The mRNA levels of target genes relative to a housekeeping gene (**Table 1)** were calculated
551 using the Livak ($2^{-\Delta\Delta Cqt}$) method. All qRT-PCR reactions for transcriptomic analysis were
552 performed in duplicate with five biological repeats for transcriptomic analysis while the
553 cytokine expression experiments were performed in triplicate with three biological repeats.
554
555 **Table 1**
556

Gene	**Primer Sequences (5′ → 3′)**
5-lo	Forward: GAGATGGCAGGGCTCGATTG Reverse: TACTCATCGGGAAGCCAGGA
cx43	Forward: GCTCTCCACTCTTTACTTCTTTCCAG Reverse: GTATTGCACTTGAAAGCTGACTGC
cxcl8a	Forward: GTCGCTGCATTGAAACAGAA Reverse: CTTAACCCATGGAGCAGAGG
cxcl8b	Forward: CTACCGAGACGTGGGTGATT Reverse: GCTCGGTGAATGGTCATTTT
cxcr2	Forward: TGACCTGCTTTTTTCCCTCACT Reverse: TGACCGGCGTGGAGGTA
cxcr1	Forward: GTGATCGTACGCGCTATGGA Reverse: ATTCGGGTTGCTAATCGCCA
tubg1	Forward: GGATACACACCGCTGACCAC Reverse: AGCCTCCTCATCACATCCAGA
rpl32	Forward: CCCTCACCAAACCTAAGATCGT Reverse: CTCCAGTTTGCCCTGATCTTG
ef1a *(housekeeping)*	Forward: AAGGAGAAGATCGACCGTCG Reverse: TGATTGAGGGAAATTCACTTGG
cxcl18b	Forward: TGCCAGTGTGAAGAGTCATC Reverse: TCGCAGTTTGGTCTTTTAGGG
il6	Forward: AGACGAGCAGTTTGAGAGAGATT Reverse: GTTTGAGGAGAGGAGTGCTGAT
il1b	Forward: ATCAAACCCCAATCCACAGAGT

	Reverse: GGCACTGAATCCACCACGTT

557
558
559 **Two-photon imaging and laser wounding**
560 Two photon imaging was performed in Tg(*lyz*:GCaMP6f)^{cu104} larvae or larvae from crosses
561 between Tg(*lyz*:GCaMP6f) x Tg(*lyz:*tRFP-5LO). Transgenic larvae expressing the calcium
562 indicator GCaMP6f were screened to ensure high reporter expression. Larvae exhibiting strong
563 fluorescence and normal morphology were selected for imaging and infection. Selected larvae
564 were anaesthetised and mounted in a mixture of 1.2% low-melting-point agarose (Invitrogen,
565 16520) and the medium (E3, isotonic E3, Ringer) containing 160-200 mg/L MS-222. Imaging
566 under sterile conditions was performed as as previously described[49]. For sterile imaging, larvae
567 were mounted on a 35 mm glass-bottom dish with a 14 mm microwell #1.5 coverglass. Excess
568 agarose was removed before solidification to embed the larvae in a thin layer. For infection
569 imaging, larvae were mounted in a custom-built coverslip chamber consisting of glass
570 coverslips sealing both the top and bottom of the sample onto a metallic ring. Larvae were
571 oriented laterally, and the agarose was allowed to solidify. After agarose solidification, the
572 urogenital region was exposed by carefully removing surrounding agarose under a dissecting
573 microscope using a pair of forceps, allowing bacterial access post-wounding. The chamber (for
574 infection conditions) or dishes (for sterile conditions) were filled with 1 mL or 4 mL of Ringer's
575 solution containing 160-200 mg/L MS-222 and 3×10^5 CFU/mL PAO1. For sterile conditions,
576 appropriate buffer (Ringer/ E3 or isotonic E3) was used as indicated.
577 Laser ablation and time-lapse imaging were performed on a LaVision TriM Scope multiphoton
578 microscope equipped with an electro-optic modulator for rapid power modulation. A Spectra-
579 Physics Insight DeepSee dual-line laser was tuned to 900 nm for imaging and 1,040 nm for
580 ablation, with imaging power set to ~500 mW at the specimen plane. Image acquisition was
581 controlled using ImSpector Pro software (version 5.0.284.0; LaVision Biotec, ©1998–2016).
582 Two-photon imaging was conducted with a 25×/NA 1.05 water-dipping objective. A 40 µm-
583 diameter region of interest was defined on a single superficial focal plane (240 nm/pixel, 15 µs
584 dwell time). Z-stacks (~20 planes, 2 µm step size) were acquired every 20 s. Laser wounding
585 was initiated after a 2 min pre-wound baseline, followed by 2 h of post-wound imaging. Focus
586 was maintained throughout acquisition. Image stacks were processed in Fiji using maximum-
587 intensity z-projections to generate neutrophil-swarming time-lapse videos for subsequent
588 analysis.

589

590 **Image analyses**

591

592 ***Defining maximum rate of recruitment***

593 After image acquisition, each video was manually analysed using Fiji, to determine the number
594 of cells recruited to the wound overtime. Using the number of cells recruited at set time points
595 (at 0 min, 5 min and then every 15 min), the maximum rate of recruitment's function was
596 calculated. In this, only the active recruitment timepoints were considered (i.e. if the
597 recruitment started at 15 min, the timepoints 0 and 5 min were not considered. Similarly, if the
598 recruitment of cells plateaued at later timepoints, those timepoints were not considered for the
599 calculation).

600

601 ***Defining the quadrants used for stratification of the imaging data***

602

603 For each video, a graph was generated using the logarithmic value of the absolute number of
604 PAO1 CFUs on the y-axis, and either the number of cells recruited or the rate of recruitment
605 function on the x-axis. Thresholds were set in PBS or control groups and then applied to *E. coli*
606 or 5-LO-Neu groups. The threshold for good recruitment was set to more than or equal to 10
607 cells recruited at the wound overtime. To determine fast recruitment rate, the mean of the
608 maximum recruitment rate of all experiments (PBS and *E. coli* for training and CTR and 5-LO-
609 Neu) was calculated and set as threshold. To evaluate the implication of CFU in disease
610 outcomes, a threshold CFU was set for experiments involving both trained larvae and 5-LO-
611 Neu larvae. The lowest CFU value that resulted in disease manifestations in the observed larvae
612 (disease score ≥1) was set as the threshold for the specific set of experiment. Employing the
613 mentioned parameters, we stratified the imaging data into four categories of larvae (G1, G2,
614 G3, G4).

615

616 ***Cell trajectories and Statistics***

617

618 Neutrophils were semi-automatically tracked using Imaris v8.2 (Bitplane AG, Zürich,
619 Switzerland) on 2D maximum intensity projections of the 4D time-lapse videos. All statistical
620 tests were performed in Prism10 (GraphPad Software, La Jolla, CA). The statistical test and
621 the n number are indicated in the figure legends. The error bars show standard error of the mean
622 except for bacterial burden data where error bars represent 95% confidence intervals of the

median. Where the distribution was verified as normal, outliers were removed by applying Rout test. Live imaging experiments were acquired in minimum five independent experiments. A normal distribution test was performed prior to any *t*-test statistical analyses. Normal distribution was assessed using *Shapiro-Wilk test*.

References

1. Schrope, J. H., Robertson, T. F., Sarris, M. & Huttenlocher, A. Chemical and Mechanical Regulation of Leukocyte Migration. *Cold Spring Harb. Perspect. Biol.* a041752 (2025) doi:10.1101/cshperspect.a041752.
2. Insall, R. H., Paschke, P. & Tweedy, L. Steering yourself by the bootstraps: how cells create their own gradients for chemotaxis. *Trends Cell Biol.* **32**, 585–596 (2022).
3. Stock, J., Kazmar, T., Schlumm, F., Hannezo, E. & Pauli, A. A self-generated Toddler gradient guides mesodermal cell migration. *Sci. Adv.* **8**, eadd2488 (2022).
4. Uçar, M. C., Alsberga, Z., Alanko, J., Sixt, M. & Hannezo, E. Self-generated chemotaxis of mixed cell populations. *Proc. Natl. Acad. Sci.* **122**, e2504064122 (2025).
5. Dalle Nogare, D. & Chitnis, A. B. A framework for understanding morphogenesis and migration of the zebrafish posterior Lateral Line primordium. *Mech. Dev.* **148**, 69–78 (2017).
6. Muinonen-Martin, A. J. *et al.* Melanoma Cells Break Down LPA to Establish Local Gradients That Drive Chemotactic Dispersal. *PLoS Biol.* **12**, e1001966 (2014).
7. Tweedy, L. *et al.* Seeing around corners: Cells solve mazes and respond at a distance using attractant breakdown. *Science* **369**, eaay9792 (2020).
8. Lämmermann, T. *et al.* Neutrophil swarms require LTB4 and integrins at sites of cell death in vivo. *Nature* **498**, 371–375 (2013).
9. Poplimont, H. *et al.* Neutrophil Swarming in Damaged Tissue Is Orchestrated by Connexins and Cooperative Calcium Alarm Signals. *Curr. Biol.* **30**, 2761-2776.e7 (2020).

10. Strickland, E. *et al.* Self-extinguishing relay waves enable homeostatic control of human neutrophil swarming. *Dev. Cell* **59**, 2659-2671.e4 (2024).
11. Afonso, P. V. *et al.* LTB4 Is a Signal-Relay Molecule during Neutrophil Chemotaxis. *Dev. Cell* **22**, 1079–1091 (2012).
12. Alanko, J. *et al.* CCR7 acts as both a sensor and a sink for CCL19 to coordinate collective leukocyte migration. *Sci. Immunol.* **8**, eadc9584 (2023).
13. Burn, G. L., Foti, A., Marsman, G., Patel, D. F. & Zychlinsky, A. The Neutrophil. *Immunity* **54**, 1377–1391 (2021).
14. Reátegui, E. *et al.* Microscale arrays for the profiling of start and stop signals coordinating human-neutrophil swarming. *Nat. Biomed. Eng.* **1**, 0094 (2017).
15. Ng, L. G. *et al.* Visualizing the Neutrophil Response to Sterile Tissue Injury in Mouse Dermis Reveals a Three-Phase Cascade of Events. *J. Invest. Dermatol.* **131**, 2058–2068 (2011).
16. Chtanova, T. *et al.* Dynamics of Neutrophil Migration in Lymph Nodes during Infection. *Immunity* **29**, 487–496 (2008).
17. Hopke, A. *et al.* Neutrophil swarming delays the growth of clusters of pathogenic fungi. *Nat. Commun.* **11**, 2031 (2020).
18. Saraswat, D. *et al.* Neutrophil swarming is crucial for limiting oral mucosal infection by *Candida albicans*. *J. Leukoc. Biol.* **117**, qiae239 (2025).
19. Herrero-Cervera, A., Soehnlein, O. & Kenne, E. Neutrophils in chronic inflammatory diseases. *Cell. Mol. Immunol.* **19**, 177–191 (2022).
20. Isles, H. M. *et al.* Pioneer neutrophils release chromatin within in vivo swarms. *eLife* **10**, e68755 (2021).

674 21. Khazen, R. *et al*. Spatiotemporal dynamics of calcium signals during neutrophil
675 cluster formation. *Proc. Natl. Acad. Sci.* **119**, e2203855119 (2022).
676 22. Kienle, K. *et al*. Neutrophils self-limit swarming to contain bacterial growth in vivo.
677 *Science* **372**, eabe7729 (2021).
678 23. Song, Z., Bhattacharya, S., Clemens, R. A. & Dinauer, M. C. Molecular regulation of
679 neutrophil swarming in health and disease: Lessons from the phagocyte oxidase.
680 *iScience* **26**, 108034 (2023).
681 24. Uderhardt, S., Martins, A. J., Tsang, J. S., Lämmermann, T. & Germain, R. N. Resident
682 Macrophages Cloak Tissue Microlesions to Prevent Neutrophil-Driven Inflammatory
683 Damage. *Cell* **177**, 541-555.e17 (2019).
684 25. Lämmermann, T. In the eye of the neutrophil swarm—navigation signals that bring
685 neutrophils together in inflamed and infected tissues. *J. Leukoc. Biol.* **100**, 55–63
686 (2016).
687 26. Netea, M. G. *et al*. Defining trained immunity and its role in health and disease. *Nat.*
688 *Rev. Immunol.* **20**, 375–388 (2020).
689 27. Kleinnijenhuis, J. *et al*. Bacille Calmette-Guérin induces NOD2-dependent
690 nonspecific protection from reinfection via epigenetic reprogramming of monocytes.
691 *Proc. Natl. Acad. Sci.* **109**, 17537–17542 (2012).
692 28. Quintin, J. *et al*. Candida albicans Infection Affords Protection against Reinfection via
693 Functional Reprogramming of Monocytes. *Cell Host Microbe* **12**, 223–232 (2012).
694 29. Kalafati, L. *et al*. Innate Immune Training of Granulopoiesis Promotes Anti-tumor
695 Activity. *Cell* **183**, 771-785.e12 (2020).
696 30. Kato, Y. & Kumanogoh, A. The immune memory of innate immune systems. *Int.*
697 *Immunol.* **37**, 195–202 (2025).

31. Mitroulis, I. *et al.* Modulation of Myelopoiesis Progenitors Is an Integral Component of Trained Immunity. *Cell* **172**, 147-161.e12 (2018).

32. Kaufmann, E. *et al.* BCG Educates Hematopoietic Stem Cells to Generate Protective Innate Immunity against Tuberculosis. *Cell* **172**, 176-190.e19 (2018).

33. Schlüter, T., Van Elsas, Y., Priem, B., Ziogas, A. & Netea, M. G. Trained immunity: induction of an inflammatory memory in disease. *Cell Res.* https://doi.org/10.1038/s41422-025-01171-y (2025) doi:10.1038/s41422-025-01171-y.

34. Fanucchi, S., Domínguez-Andrés, J., Joosten, L. A. B., Netea, M. G. & Mhlanga, M. M. The Intersection of Epigenetics and Metabolism in Trained Immunity. *Immunity* **54**, 32–43 (2021).

35. Darroch, H. *et al.* Infection-experienced HSPCs protect against infections by generating neutrophils with enhanced mitochondrial bactericidal activity. *Sci. Adv.* **9**, eadf9904 (2023).

36. Mariotti, B. *et al.* Innate immune reprogramming in circulating neutrophils of COPD patients. *J. Allergy Clin. Immunol.* **156**, 373–384 (2025).

37. Gomes, M. C., Brokatzky, D., Bielecka, M. K., Wardle, F. C. & Mostowy, S. *Shigella* induces epigenetic reprogramming of zebrafish neutrophils. *Sci. Adv.* **9**, eadf9706 (2023).

38. Patel, K. K., Tariveranmoshabad, M., Kadu, S., Shobaki, N. & June, C. From concept to cure: The evolution of CAR-T cell therapy. *Mol. Ther.* **33**, 2123–2140 (2025).

39. Abdin, S. M., Paasch, D. & Lachmann, N. CAR macrophages on a fast track to solid tumor therapy. *Nat. Immunol.* **25**, 11–12 (2024).

40. Chang, Y. *et al.* CAR-neutrophil mediated delivery of tumor-microenvironment responsive nanodrugs for glioblastoma chemo-immunotherapy. *Nat. Commun.* **14**, 2266 (2023).
41. Chang, Y. *et al.* Engineering chimeric antigen receptor neutrophils from human pluripotent stem cells for targeted cancer immunotherapy. *Cell Rep.* **40**, 111128 (2022).
42. Majumder, A. *et al.* iPSC-Derived CAR Neutrophils Possess Potent Activity Against Solid Tumors In Vivo. *Blood* **144**, 86–86 (2024).
43. Sathe, N. *et al.* Pseudomonas aeruginosa: Infections and novel approaches to treatment "Knowing the enemy" the threat of Pseudomonas aeruginosa and exploring novel approaches to treatment. *Infect. Med.* **2**, 178–194 (2023).
44. Ruffin, M. & Brochiero, E. Repair Process Impairment by Pseudomonas aeruginosa in Epithelial Tissues: Major Features and Potential Therapeutic Avenues. *Front. Cell. Infect. Microbiol.* **9**, 182 (2019).
45. Clatworthy, A. E. *et al.* *Pseudomonas aeruginosa* Infection of Zebrafish Involves both Host and Pathogen Determinants. *Infect. Immun.* **77**, 1293–1303 (2009).
46. Gault, W. J., Enyedi, B. & Niethammer, P. Osmotic surveillance mediates rapid wound closure through nucleotide release. *J. Cell Biol.* **207**, 767–782 (2014).
47. Enyedi, B., Kala, S., Nikolich-Zugich, T. & Niethammer, P. Tissue damage detection by osmotic surveillance. *Nat. Cell Biol.* **15**, 1123–1130 (2013).
48. Huang, C. & Niethammer, P. Tissue Damage Signaling Is a Prerequisite for Protective Neutrophil Recruitment to Microbial Infection in Zebrafish. *Immunity* **48**, 1006-1013.e6 (2018).

744 49. Williantarra, I., Georgantzoglou, A. & Sarris, M. Visualising Neutrophil Actin Dynamics
745 in Zebrafish in Response to Laser Wounding Using Two-Photon Microscopy. *BIO-*
746 *Protoc.* **14**, (2024).
747 50. LaBauve, A. E. & Wargo, M. J. Growth and Laboratory Maintenance of *Pseudomonas*
748 *aeruginosa*. *Curr. Protoc. Microbiol.* **25**, (2012).
749 51. Potvin-Trottier, L., Lord, N. D., Vinnicombe, G. & Paulsson, J. Synchronous long-term
750 oscillations in a synthetic gene circuit. *Nature* **538**, 514–517 (2016).
751 52. Park, S. A., Choe, Y. H., Park, E. & Hyun, Y.-M. Real-time dynamics of neutrophil
752 clustering in response to phototoxicity-induced cell death and tissue damage in
753 mouse ear dermis. *Cell Adhes. Migr.* 1–20 (2018)
754 doi:10.1080/19336918.2018.1471322.
755 53. Horn, A. *et al.* Isotonic medium treatment limits burn wound microbial colonisation
756 and improves tissue repair. *Wound Repair Regen.* **33**, e13242 (2025).
757 54. Kazmierczak, B. I., Schniederberend, M. & Jain, R. Cross-regulation of Pseudomonas
758 motility systems: the intimate relationship between flagella, pili and virulence. *Curr.*
759 *Opin. Microbiol.* **28**, 78–82 (2015).
760 55. Huang, L. *et al.* Engineered probiotic Escherichia coli elicits immediate and long-term
761 protection against influenza A virus in mice. *Nat. Commun.* **15**, 6802 (2024).
762 56. Moorlag, S. J. C. F. M. *et al.* Multi-omics analysis of innate and adaptive responses to
763 BCG vaccination reveals epigenetic cell states that predict trained immunity.
764 *Immunity* **57**, 171-187.e14 (2024).
765 57. Wang, W. *et al.* Breakthrough of solid tumor treatment: CAR-NK immunotherapy. *Cell*
766 *Death Discov.* **10**, 40 (2024).

58. Sterner, R. C. & Sterner, R. M. CAR-T cell therapy: current limitations and potential strategies. *Blood Cancer J.* **11**, 69 (2021).

59. Bradford, Y. M. *et al.* Zebrafish information network, the knowledgebase for *Danio rerio* research. *Genetics* **220**, iyac016 (2022).

60. Renshaw, S. A. *et al.* A transgenic zebrafish model of neutrophilic inflammation. *Blood* **108**, 3976–3978 (2006).

61. Bakshi, S. *et al.* Tracking bacterial lineages in complex and dynamic environments with applications for growth control and persistence. *Nat. Microbiol.* **6**, 783–791 (2021).

62. Sarris, M. *et al.* Inflammatory Chemokines Direct and Restrict Leukocyte Migration within Live Tissues as Glycan-Bound Gradients. *Curr. Biol.* **22**, 2375–2382 (2012).

Figure Legends

FIGURE_1

A. Schematic detailing the mechanical wound (MW) wound-infection model by tail fin (TF) transection method in the presence of *P. aeruginosa* PAO1.
B. Parameters assessed in the disease scoring matrix to accord a disease progression stage to each zebrafish larva.
C. Disease progression in the specified group of larvae at the indicated time points. Representative of three independent experiments, with n ≥ 24 larvae per group.
D. Bacterial burden of *P. aeruginosa* in the specified groups of zebrafish larvae at 24 hpi (hours post infection). CFU, colony forming units. (Representative of three independent experiments with n ≥9 larvae per group used for CFU analysis in each experiment). (mean ± SD). *One-way ANOVA with Tukey's multiple comparisons test,* ***$P < 0.001$
E. Survival curves from zebrafish larvae when exposed to indicated buffers and *P. aeruginosa* infection upon MW. (Representative of three independent experiments with n ≥ 24 larvae per group for the wounded-infected; n ≥ 9 larvae per group for the non-wounded infected, in each experiment). *Log-rank (Mantel-Cox) test; ***$P < 0.001$*
F. Bacterial burden of *P. aeruginosa* in the specified groups of zebrafish larvae at early time points (10 mins and 30 mins) of infection. (Representative of three independent experiments with n ≥ 12 larvae per group per time point in each experiment. (mean ± SD). CFU, colony forming units. *One-way ANOVA with, Šídák's multiple comparisons test,* **$P < 0.01$
G. Schematic detailing the laser wound (LW) infection model. CHT: caudal hematopoietic tissue; VF: ventral fin.
H. Survival curves from zebrafish larvae when exposed to indicated buffers and *P. aeruginosa* infection upon LW. (Representative of three independent experiments with n ≥ 24 larvae per group for the wounded-infected; n≥12 larvae per group for the non-wounded infected, in each experiment). *Log-rank (Mantel-Cox) test,* *$P < 0.05$
I. Bacterial burden of *P. aeruginosa* in the specified groups of zebrafish larvae at 24 hpi (hours post infection). Representative of three independent experiments, with n ≥12 larvae per group in each experiment. (mean ± SD). CFU, colony forming units. *Unpaired t test,* *$P < 0.05$*

814 J. Disease progression in the specified group of larvae at the indicated time points.
815 Representative of three independent experiments with n ≥ 24 larvae per group.
816
817 **FIGURE _2**
818
819 A. Schematic of the training experiment. Zebrafish larvae pre-challenged by PBS or a dose
820 of *E. coli* in the otic vesicle (OV) at 2 days post fertilization (dpf) stage and
821 subsequently subjected to mechanical wounding in the tail fin (TF) and *P. aeruginosa*
822 PAO1 infection at 4 dpf.
823 B. Survival curves from control (PBS) and trained (EC) zebrafish larvae upon *P.*
824 *aeruginosa* infection following MW. (Representative of three independent experiments
825 with n ≥ 36 larvae per group in each experiment). *Log-rank (Mantel-Cox) test; ****P*
826 *< 0.0001.*
827 C. Bacterial burden of *P. aeruginosa* in the control and trained zebrafish larvae at 24 hpi
828 (hours post infection). (Representative of three independent experiments, with n ≥ 9
829 larvae per group used for CFU analysis in each experiment. (mean ± SD). CFU, colony
830 forming units. *One-way ANOVA with Tukey's multiple comparisons test, *P < 0.05*
831 D. Disease progression in the control and trained zebrafish larvae at the indicated time
832 points. Representative of three independent experiments with n ≥ 36 larvae per group
833 in each experiment.
834 E. Schematic detailing the assessment of *E. coli* burden and cytokine profile in whole
835 zebrafish larvae after primary challenge (PBS/ *E. coli*) for trained immunity induction.
836 F. Bacterial counts at the indicated time points after injection of *E. coli* in the otic vesicle
837 (OV) of the zebrafish larvae. Representative of three independent experiments, with n
838 ≥ 12 larvae for each time point.
839 G-J. Change in the expression profile of the indicated cytokines in naive and trained
840 zebrafish larvae at the specific time points after primary challenge. Representative of
841 three independent experiments, with n ≥ 8 larvae at each time point.
842 K. Schematic describing the isolation of neutrophils by Fluorescence Activated Cell
843 Sorting (FACS) from the hematopoietic site (CHT: Caudal hematopoietic tissue) of
844 zebrafish larvae, followed by transcript analysis using RT-PCR.
845 L-R. Change in the expression profile of the indicated genes in naive and trained zebrafish
846 larvae at 4dpf (2 days after primary challenge). Quantitative PCR data are presented as
847 mean ± S.E.M., with expression levels normalised to PBS-treated control groups (n=5

848 independent experiments, with each replicate representing a pool of 150-200 larvae at
849 4 dpf). Statistical significance was assessed using the Mann-Whitney test/ t-test (*p <
850 0.05, **p < 0.01).
851
852 **FIGURE_3**
853
854 A. Schematic of experiment with control, PBS pre-challenged or trained, *E. Coli* pre-
855 challenged (EC) zebrafish larvae subjected to laser wounding (LW), followed by
856 infection with *P. aeruginosa* (PAO1) and simultaneous confocal imaging.
857 B. Time lapse images of representative videos of control and trained larvae at 1 min prior
858 LW (-1 min), at the time of LW (0 min), at 30 min and 90 min post LW. White dashed
859 lines correspond to the CHT: caudal hematopoietic tissue and VF: ventral fin. Red
860 dashed lines correspond to the site of the LW. On the far-right, neutrophil trajectories
861 of same video are depicted wherein each colour corresponds to a different neutrophil
862 trajectory. Scale bar 50 µm.
863 C. Summary of individual larva-based analyses of control (PBS) *(left)* and trained (EC)
864 animals *(right)*. The y-axis on the graph depicts bacterial burden in larva at 24 hours
865 post infection (hpi) (after LW and infection), and the x-axis indicates cumulative
866 number of neutrophils recruited at 120 minutes post LW. Thresholds are set at the
867 minimum PAO1 CFU value in which disease symptoms were observed (stage 1 or
868 above, light blue square), and 10 neutrophils recruited over time. Black arrows point to
869 videos used for representative images in B (PBS example 1= PBS G1; PBS example 2=
870 PBS G2; EC example 1= EC G2; EC example 2= EC G3). Different shapes and colour
871 show the individual disease stages of each larva.
872 D. Contingency analysis of groups in C. n=16 (PBS) and n=17 (EC). *Fisher's exact test **
873 *p < 0.05.*
874 E-F. Survival curves from control (PBS) and trained (EC) zebrafish larvae upon PAO1
875 infection following mechanical wound. Larvae were pre-treated with DMSO or 20µM
876 Zileuton (Zil), 1h prior to wounding and kept in this medium until the end of the
877 experiment Representative of three independent experiments with n ≥28 larvae per
878 group for each experiment in E, and n ≥ 20 larvae in F. *Log-rank (Mantel-Cox) test; **
879 *p < 0.05 , ns p > 0.05.*
880 G-H. Bacterial burden of *P. aeruginosa* in larvae from groups in E and F respectively.
881 Representative of three independent experiments with n ≥ 9 larvae per group used for

882 CFU analysis in each experiment. (mean ± SD). CFU, colony forming units. *Unpaired*
883 *t test with Welch's correction. * $p < 0.05$, ns $p > 0.05$.*
884
885 **FIGURE_4**
886
887 A. Survival curves from control (CTR) zebrafish larvae and larvae overexpressing 5-LO
888 in neutrophils (5-LO-Neu) upon *P. aeruginosa* infection following MW.
889 Representative of three independent experiments with n ≥ 50 larvae per group in each
890 experiment. *Log-rank (Mantel-Cox) test; * $p < 0.05$.*
891 B. Bacterial burden of fish in survival experiments (A). Representative of three
892 independent experiments with n ≥ 9 larvae per group used for CFU analysis in each
893 experiment. *Unpaired t test with Welch's correction; * $p < 0.05$, ** $p < 0.01$.*
894 C. Disease progression in the specified group of larvae at the indicated time points.
895 Representative of three independent experiments with n ≥ 50 larvae per group in each
896 experiment.
897 D. Time lapse images of representative videos of CTR and 5-LO-Neu at 1 min prior to LW
898 (-1 min), at the time of LW (0 min), at 30 min and 90 min after LW. White dashed lines
899 indicated the CHT: caudal hematopoietic tissue and VF: ventral fin. Red dashed line
900 corresponds to the site of the laser wound (LW). On the right column neutrophil
901 trajectories of same video are represented wherein each colour indicates a different
902 neutrophil trajectory. Scale bar 50 µm.
903 E. Summary of individual larva-based analyses of control (CTR) larvae (*left)* and 5-LO-
904 Neu larvae *(right)*. The y-axis on the graph depicts bacterial burden PAO1 in larva at
905 24 hours post infection (hpi) (after LW and infection), and the x-axis indicates the
906 maximum rate of neutrophil recruitment. Thresholds are set at the minimum CFU value
907 in which disease symptoms were observed (stage 1, light blue square) and the mean of
908 maximum rate of recruitment for both CTR and 5-LO-Neu experiments. Black arrows
909 point to videos used for representative images in (D) (arrow in CTR example 1= CTR
910 G1, CTR example 2=CTR G2; 5-LO- example 1=5-LO-Neu G2, 5-LO-Neu example
911 2=5-LO-Neu G3). Different shapes and colour show disease stages of individual larva.
912 Videos of larva wherein recruiting cells were observed at only one time point were
913 excluded.
914 F. Contingency analysis of groups in E. n=15 (CTR) and n=18 (5LO). *Fisher's exact test*
915 ** $p < 0.05$.*

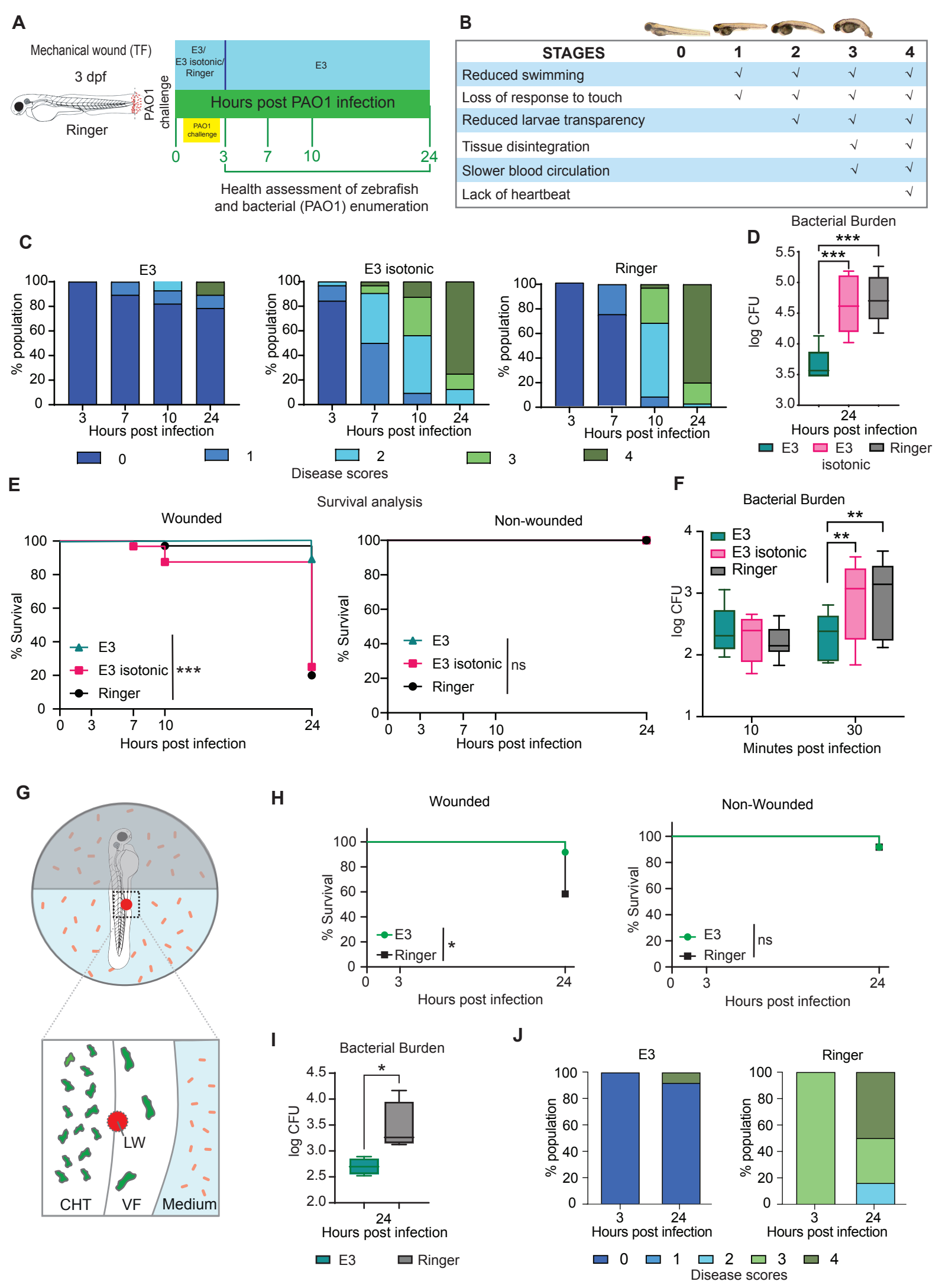
A
Mechanical wound (TF)
3 dpf
Ringer
PAO1 challenge
E3/ E3 isotonic/ Ringer
E3
Hours post PAO1 infection
PAO1 challenge
0
3
7
10
24
Health assessment of zebrafish and bacterial (PAO1) enumeration
B
STAGES 0 1 2 3 4
Reduced swimming √ √ √ √
Loss of response to touch √ √ √ √
Reduced larvae transparency √ √ √
Tissue disintegration √ √
Slower blood circulation √ √
Lack of heartbeat √
C
E3
E3 isotonic
Ringer
% population
Hours post infection
Disease scores
D
Bacterial Burden
log CFU
Hours post infection
E3
E3 isotonic
Ringer
E
Survival analysis
Wounded
Non-wounded
% Survival
Hours post infection
E3
E3 isotonic
Ringer
***
ns
F
Bacterial Burden
log CFU
Minutes post infection
G
CHT
VF
Medium
LW
H
Wounded
Non-Wounded
% Survival
Hours post infection
E3
Ringer
*
ns
I
Bacterial Burden
log CFU
Hours post infection
E3
Ringer
J
E3
Ringer
% population
Hours post infection
Disease scores

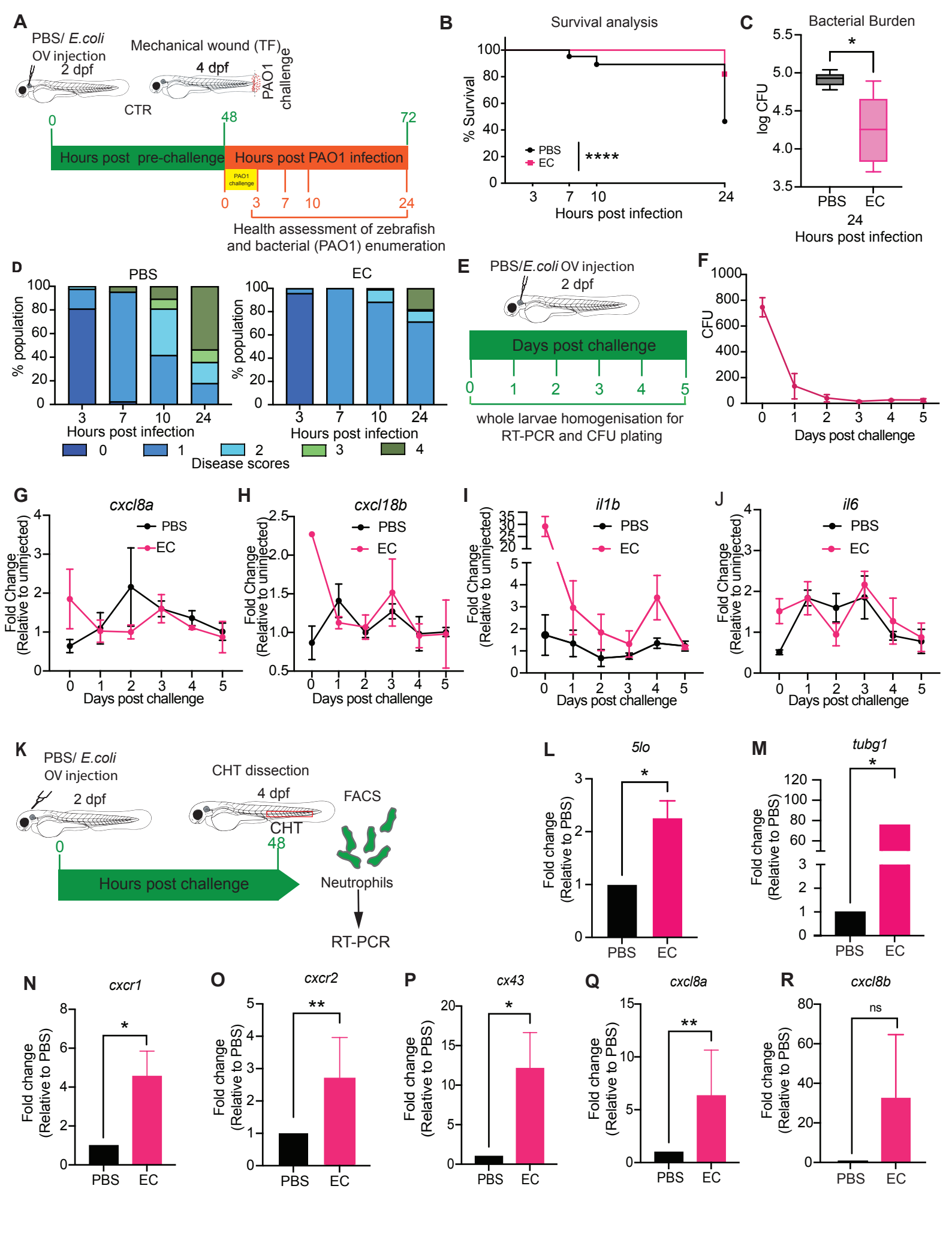
A
PBS/ E.coli
OV injection
2 dpf
Mechanical wound (TF)
4 dpf
PAO1
challenge
CTR
0
48
72
Hours post pre-challenge
Hours post PAO1 infection
PAO1 challenge
0 3 7 10 24
Health assessment of zebrafish and bacterial (PAO1) enumeration
B
Survival analysis
% Survival
PBS
EC
****
Hours post infection
C
Bacterial Burden
log CFU
PBS
EC
24
Hours post infection
D
PBS
EC
% population
Hours post infection
Disease scores
E
PBS/E.coli OV injection
2 dpf
Days post challenge
whole larvae homogenisation for RT-PCR and CFU plating
F
CFU
Days post challenge
G
cxcl8a
Fold Change (Relative to uninjected)
Days post challenge
H
cxcl18b
I
il1b
J
il6
K
PBS/ E.coli
OV injection
2 dpf
CHT dissection
4 dpf
CHT
FACS
Hours post challenge
Neutrophils
RT-PCR
L
5lo
Fold change (Relative to PBS)
M
tubg1
N
cxcr1
O
cxcr2
P
cx43
Q
cxcl8a
R
cxcl8b
ns

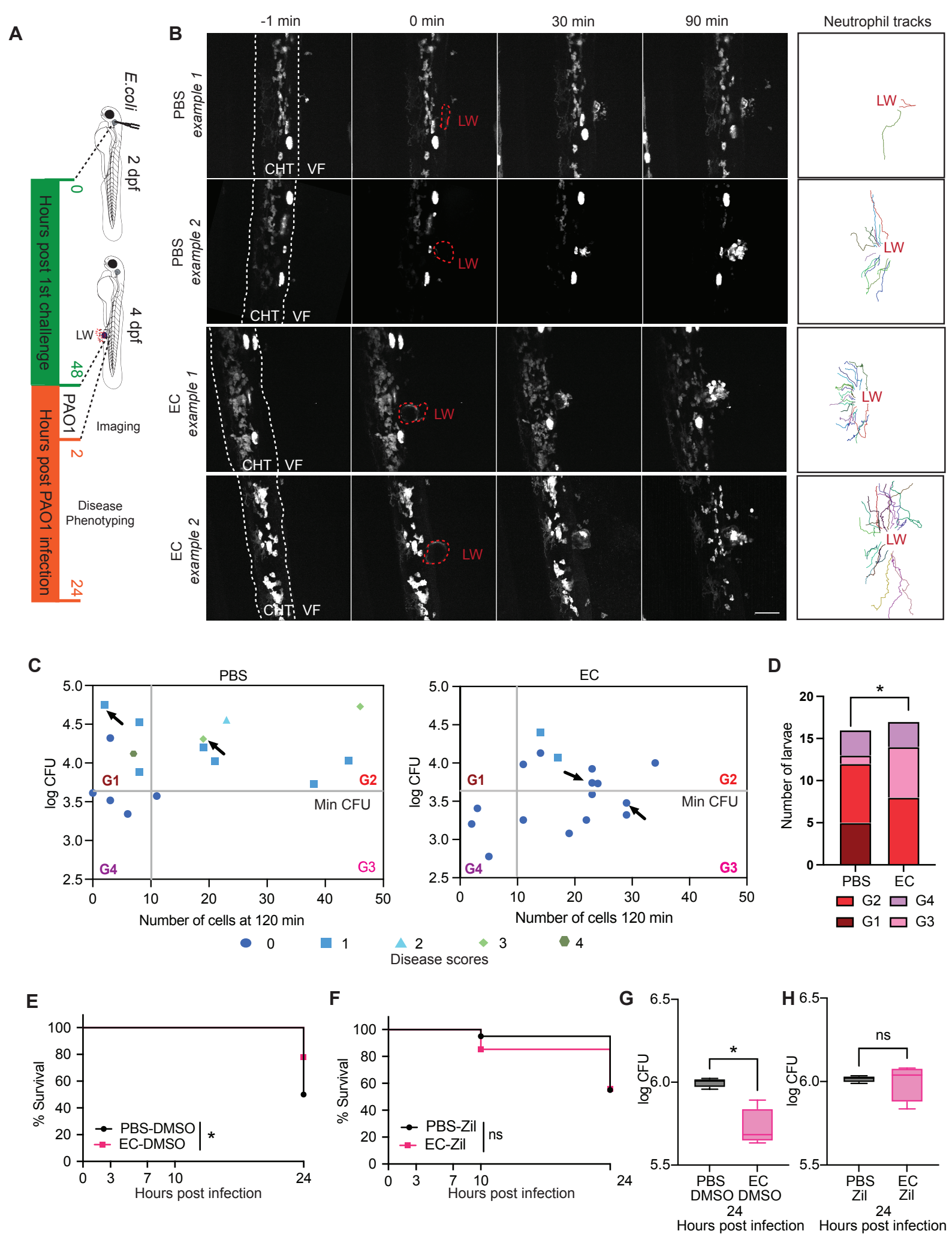
A
E.coli
2 dpf
4 dpf
LW
0
48
PAO1
2
24
Hours post 1st challenge
Hours post PAO1 infection
Imaging
Disease Phenotyping
B
-1 min
0 min
30 min
90 min
Neutrophil tracks
PBS example 1
PBS example 2
EC example 1
EC example 2
CHT
VF
LW
C
PBS
EC
log CFU
Number of cells at 120 min
Number of cells 120 min
Min CFU
G1
G2
G3
G4
Disease scores
D
Number of larvae
PBS
EC
G2
G4
G1
G3
E
% Survival
PBS-DMSO
EC-DMSO
Hours post infection
F
PBS-Zil
EC-Zil
ns
G
log CFU
PBS DMSO
EC DMSO
24 Hours post infection
H
PBS Zil
EC Zil

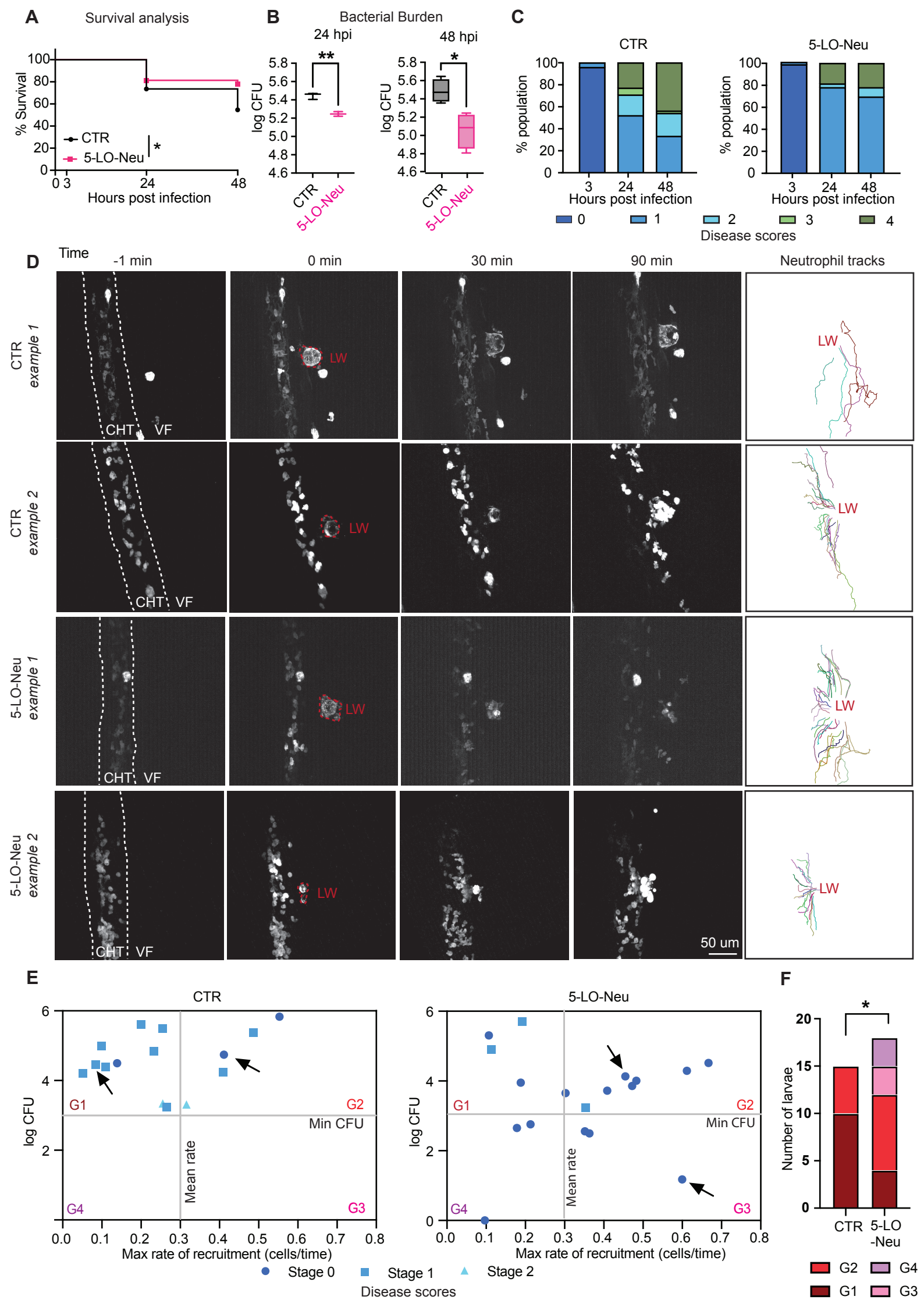
A
Survival analysis
% Survival
CTR
5-LO-Neu
*
Hours post infection
B
Bacterial Burden
24 hpi
48 hpi
log CFU
**
*
CTR
5-LO-Neu
C
CTR
5-LO-Neu
% population
Hours post infection
Disease scores
D
Time
-1 min
0 min
30 min
90 min
Neutrophil tracks
CTR example 1
CTR example 2
5-LO-Neu example 1
5-LO-Neu example 2
CHT
VF
LW
50 um
E
CTR
5-LO-Neu
log CFU
Max rate of recruitment (cells/time)
G1
G2
G3
G4
Min CFU
Mean rate
Stage 0
Stage 1
Stage 2
Disease scores
F
Number of larvae
CTR
5-LO -Neu
G2
G4
G1
G3